
# A comparative DFT study of the mechanical and electronic properties of greigite Fe3S4 and magnetite Fe3O4

A. Roldan, D. Santos-Carballal, and N. H. de Leeuw

Citation: J. Chem. Phys. **138**, 204712 (2013); doi: 10.1063/1.4807614
View online: http://dx.doi.org/10.1063/1.4807614
View Table of Contents: http://jcp.aip.org/resource/1/JCPSA6/v138/i20
Published by the American Institute of Physics.

# A comparative DFT study of the mechanical and electronic properties of greigite $Fe_3S_4$ and magnetite $Fe_3O_4$

A. Roldan,[a] D. Santos-Carballal, and N. H. de Leeuw
*Department of Chemistry, University College London, London WC1H 0AJ, United Kingdom*

(Received 4 March 2013; accepted 9 May 2013; published online 30 May 2013)

Greigite ($Fe_3S_4$) and its analogue oxide, magnetite ($Fe_3O_4$), are natural minerals with an inverse spinel structure whose atomic-level properties may be difficult to investigate experimentally. Here, [D. Rickard and G. W. Luther, Chem. Rev. **107**, 514 (2007)] we have calculated the elastic constants and other macroscopic mechanical properties by applying elastic strains on the unit cells. We also have carried out a systematic study of the electronic properties of $Fe_3S_4$ and $Fe_3O_4$, where we have used an *ab initio* method based on spin-polarized density functional theory with the on-site Coulomb repulsion approximation ($U_{eff}$ is 1.0 and 3.8 eV for $Fe_3S_4$ and $Fe_3O_4$, respectively). Comparison of the properties of $Fe_3S_4$ and $Fe_3O_4$ shows that the sulfide is more covalent than the oxide, which explains the low magnetization of saturation of greigite cited in several experimental reports. © *2013 AIP Publishing LLC*. [http://dx.doi.org/10.1063/1.4807614]

## I. INTRODUCTION

Metal sulfides have been known and used as a source of metals since ancient times. They constitute the most important group of ore minerals, making them the raw materials of choice for most of the world production of non-ferrous metals. Sulfides of iron, the most abundant transition element in the Earth's crust, occur frequently with Fe and S in different oxidation states, yielding various types of natural iron sulfides. In the present oxidized ocean, for instance, iron sulfides can be found in environments rich in Fe and S such as sedimentary pore waters and deep waters of anoxic basins.[1] In general, iron sulfide minerals display interesting magnetic and electrical properties, which are strongly related to the stoichiometric ratio between Fe and S atoms and their crystalline structure. These minerals are classified according to their Fe:S ratio as marcasite or pyrite ($0.5 < \text{Fe:S} < 1.05$), greigite ($Fe_3S_4$), pyrrhotite, troilite, or mackinawite ($Fe_{1-x}S$: $0 < x < 0.125$; $x = 0$ or $-0.05 < x < 0.0$, respectively).

Greigite is formed as an intermediate in the solid-state transformation of mackinawite into pyrite, playing a crucial role in the pyrite formation pathway.[2–5] The model for the mackinawite-greigite transition proposed by Lennie *et al.*[6] requires the diffusion of approximately two of every four $Fe^{2+}$ cations from tetrahedral sites in mackinawite to octahedral sites in $Fe_3S_4$, with the concomitant oxidation of half the migrating $Fe^{2+}$ to $Fe^{3+}$. The solid-state transformation of $Fe_3S_4$ into pyrite requires the outward diffusion of tetrahedral Fe, the reduction of $Fe^{3+}$, and the oxidation of sulfide to disulfide.[3,6] Nevertheless, although $Fe_3S_4$ is not the most stable iron sulfide structure, it has been widely identified in marine soils and sedimentary rocks of up to a few million years old (Ref. 7 and references therein). Moreover, some bacteria in anoxic marine environments produce greigite, where it has been associated as a catalyst in a number of key biochemical reactions associated with the "iron-sulfur world" hypothesis for the origin of life.[8–11]

It is of significant research interest that $Fe_3S_4$ is a rare inverse spinel mineral and isomorphic with the iron oxide magnetite ($Fe_3O_4$). Its cubic unit cell consists of eight $Fe_3S_4$ subunits with a lattice parameter of ~9.8 Å.[12,13] The inverse spinel arrangement is reflected by the formula $Fe^{3+}(Fe^{3+}Fe^{2+})S_4$, where there are two possible locations for the Fe ions: the tetrahedral sites, filled by $Fe^{3+}$ ions, and the octahedral sites, where both $Fe^{3+}$ and $Fe^{2+}$ ions reside (Fig. 1).[14–18] Mössbauer experiments[14,19] and spin-polarized multiple-scattering calculations[20–22] have shown high-spin electronic configurations for both Fe sites with the effective spin in octahedral sites higher than in tetrahedral ones.[23] The orbital spin-splitting in the valence region results in localized outermost *3d*-electrons and in ordered magnetism.[1,14,17] The spins in tetrahedral and octahedral Fe are aligned antiparallel with respect to each other, indicating ferrimagnetic and semiconducting properties unlike other spinels.[14–16,19,23] $Fe_3S_4$ magnetization of saturation has been reported, as well as the *Curie* temperature, in a wide range of values for both natural and synthetic samples. It is due to the presence of non-ferrimagnetic impurities, sample oxidation (even in an argon environment), or its decomposition at high temperatures.[1,16,24] In addition, the particle size is important for magnetism measurements, as the particle size determines the contribution of the external shell in relation to the bulk-core, where ultrafine magnetic particles produce superparamagnetic behaviour.[25]

In the present paper, we have used DFT+U methodology to report intrinsic and mechanical properties of $Fe_3S_4$, including its elastic constants, and compared these with the same properties of $Fe_3O_4$. The elastic constants provide important information concerning the nature of the forces operating in the solids and form a link between mechanical and

[a]Author to whom correspondence should be addressed. Electronic mail: alberto.roldan@ucl.ac.uk. Fax: +44 (0)20 7679 7463.

 

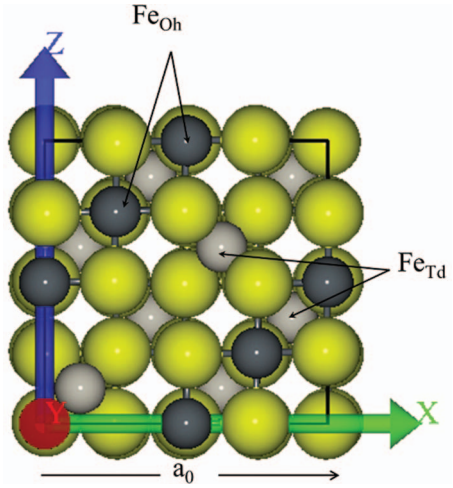


FIG. 1. Schematic representation of the spinel structure, where tetrahedral Fe ($Fe_{Td}$) atoms are pale-grey balls, octahedral Fe ($Fe_{Oh}$) are dark-grey balls, and S or O atoms are dark-yellow balls.

dynamical properties. These properties predict a more covalent character for $Fe_3S_4$ than for $Fe_3O_4$, whereas we also explain the failure of the Néel model[26] to predict $Fe_3S_4$ magnetic moments.

## II. COMPUTATIONAL DETAILS

We have used the Vienna Ab initio Simulation Package (VASP) code to carry out spin-polarized calculations within the usual Kohn-Sham (KS) implementation of density functional theory (DFT).[27,28] The generalized gradient approximation (GGA) was employed with the PW91 functional,[29] with the spin interpolation formula of Vosko *et al.*[30] and dispersion interactions correction via the semiempirical method of Grimme.[31] The inner electrons consisting of orbitals up to, and including, the 3*p* levels for Fe, the 2*p* level for S, and the *1s* for O, were described by the projector augmented wave (PAW) method.[32] KS valence states were expanded in a plane-wave basis set with a cut off at 600 eV and 520 eV for the kinetic energy of sulfide and oxide, respectively, these high values ensured that no Pulay stresses occurred within the cell during relaxations. An energy threshold defining self-consistency of the electron density was set to $10^{-5}$ eV. In order to improve the convergence of the Brillouin-zone integrations, the partial occupancies were determined using the tetrahedron method with Blöchl corrections, with a set width for all calculations of 0.02 eV. These smearing techniques can be considered as a form of finite-temperature DFT,[33] where the varied quantity is the electronic free energy, however, final energy values were corrected to 0 K (no smearing). The optimization of the structures was conducted via a conjugate gradients technique, which uses the total energy and the Hellmann-Feynman forces on the atoms, where in the present paper the break condition for the ionic relaxation loop was set at 0.01 eV/Å. Spin-orbit coupling was not considered as its influence is negligible on the atomic magnetic moments.[34]

Within the VASP code, it is possible to assign an initial spin population and orientation at each atom, where the system will converge to the ground state spin configuration, but keeping the same orientation on the spins. Thus, the initial magnetic moment was described by a high spin ferrimagnetic distribution on both types of Fe. However, to describe the magnetic behaviour properly, an accurate treatment of the electron correlation in the localized *d*-Fe orbitals is crucial. Hence, we have used the Hubbard approximation[35,36] to improve the description of localized states in this type of system, where standard local-density approximation (LDA) and GGA functionals fail.[37] The disadvantage of this approximation is the rather empirical character of the $U_{eff}$ parameter choice, a feature that also appears when using hybrid functionals since the amount of Fock exchange is system-dependent.[37–41] Therefore, we have followed the approach used by Devey *et al.*[22] who determined a suitable $U_{eff}$ value for $Fe_3S_4$ at $U_{eff} = 1$ eV, which was chosen on the basis of comparison of the computed lattice parameters and band gap with the available experimental data.[42] For $Fe_3O_4$, we fitted the $U_{eff}$ vs. the band gap in the low-symmetry unit cell, below the Verwey temperature,[43] which presents a non-metallic character shown by a small band gap of ~0.14 eV.[44–46] As we found that $U_{eff} = 3.8$ eV opens a band gap of 0.14 eV, we have considered $U_{eff} = 3.8$ eV in the 56 atoms high-symmetry unit cell, by modifying the same orbitals as in $Fe_3S_4$.

Bulk calculations were carried out on a spinel cubic cell containing 56 atoms, of which 24 were Fe atoms and 32 were S atoms (or O atoms in the $Fe_3O_4$ case) (Fig. 1). All atoms were fully relaxed until the required accuracy was reached. Calculations were carried out in the reciprocal space of the cell and were described by a Monkhorst-Pack grid[47] of 4 × 4 × 4 k-points, which ensures the electronic and ionic convergence. Higher numbers of k-points were tested but these led to an energy difference of less than 0.01 eV.

The elastic tensors were determined using the standard finite difference technique, where the calculation of the second order elastic constants is achieved through the description of a linear elastic strain response of the material as it opposes to a certain stress. Each elastic constant ($C_{ij}$) is a component of a matrix, denoted by Voigt notation as subscript. We have derived each $C_{ij}$ via the second-order Taylor expansion of the total energy with respect to the applied distortion, Eq. (1), where E is the total energy of the stressed cell, $\varepsilon$ is the component of the applied strain, and V is the equilibrium volume,[48,49]

$$C_{ij} = \frac{1}{V}\frac{\partial^2 E}{\partial \varepsilon_i \partial \varepsilon_j}. \quad (1)$$

We have optimized both the lattice parameters and the internal atomic coordinates to avoid residual stresses, which are essential in the performance of an accurate comparison. The strain applied was up to ±0.4% of the cell parameter keeping a constant volume as describe by Ainsworth *et al.*[49] Due to the crystal symmetry, the minimum linearly independent sets of strains to determine the elastic constants are two, leading to the $C_{11}$, $C_{12}$, and $C_{44}$ matrix components. For less symmetric crystals, such as orthorhombic, monoclinic, or triclinic, space groups up to six sets need to be determined.

## III. RESULTS AND DISCUSSION

### A. Structural properties

After geometry optimization, the calculated cubic cell parameters are 9.671 and 8.390 Å for $Fe_3S_4$ and $Fe_3O_4$, respectively, the experimental value for $Fe_3O_4$ is 8.390405.[43] Both parameters are in good agreement with the experiment (see Table I for $Fe_3S_4$) considering that GGA functionals typically underestimate the structural properties of strongly correlated magnetic systems, including metal oxides and sulfides, due to the underestimation of exchange-splitting.[50] The mean distance between octahedral Fe and surrounding S atoms is $d(Fe_{Oh}–S) = 2.37$ Å, slightly larger than for tetrahedral Fe $d(Fe_{Td}–S) = 2.18$ Å, with both distances differing less than 0.1 Å from reported measurements.[18,51] As expected, both distances are longer in greigite than in magnetite, where the mean distances are $d(Fe_{Oh}–O) = 2.05$ Å and $d(Fe_{Td}–O) = 1.89$ Å, differing less than 0.01 Å from previously reported distances.[52] We carried out Bader analysis to obtain the arrangement of charge and spin densities along the unit cells, which, considering the electron delocalization by using DFT, do not provide enough information to determine the electronic structure and supplementary techniques as density of states (DOS) are required. Structural data of $Fe_3S_4$ and $Fe_3O_4$ is summarised in Table II. We have also carried out a DFPerturbation theory[53] calculation with fully relaxed cell vectors and ionic coordinates to obtain the phonon vibrations, where the 3N vibrational frequencies range between 385–59 $cm^{-1}$ and 674–142 $cm^{-1}$ for $Fe_3S_4$ and $Fe_3O_4$, respectively.

### B. Mechanical properties

An accurate experimental determination of elastic constants needs large pure single crystals that are difficult to obtain, and it is hence not surprising that no information about the mechanical properties of $Fe_3S_4$ is available in the literature. Nevertheless, a comparison with the known $Fe_3O_4$ properties may validate our calculated results. For this purpose, we have derived the elastic constants $C_{11}$, $C_{12}$, and $C_{44}$ of both the $Fe_3S_4$ and $Fe_3O_4$ cubic cells. These elastic constants, summarised in Table III, quantify the response of the crystal to external forces, and are related to macroscopic parameters obtained from an average of randomly oriented polycrystals.

The elastic constant $C_{11}$ (and equivalent: $C_{22}$ and $C_{33}$) measures the response of the cell to a pressure applied perpendicular to each cell face. $C_{11}$ is calculated at 105 and 242 GPa for $Fe_3S_4$ and $Fe_3O_4$, respectively (Table III). The calculated value of $C_{11}$ is clearly higher for $Fe_3O_4$ than for $Fe_3S_4$, with the $C_{11}$ of $Fe_3O_4$ fairly close to the accepted experimental value of 260.5 GPa. This early result corroborates the suggestion that sulfide is easier to compress (softer) than the oxide.[61] A distortion along two different axes leads to $C_{12}$, $C_{21}$, $C_{23}$, and $C_{32}$, which are equivalent elastic constants. The calculated $C_{12}$ for $Fe_3O_4$ differs less than 19 GPa from the experimental value while $C_{12}(Fe_3S_4)$ is 42 GPa. For the last independent elastic constant, $C_{44}$, we obtain a value of 39 and 55 GPa, respectively, for the sulfide and the oxide. The calculated elastic constants for $Fe_3O_4$ compare well with the experimental benchmark,[61] and with a maximum discrepancy of 13% in $Fe_3O_4$, we might expect an equally good prediction for the calculated elastic constants of $Fe_3S_4$.

We have calculated the $Fe_3S_4$ and $Fe_3O_4$ bulk and shear moduli by equating the uniform strain in the crystal aggregates to the external isostrain in the Voigt approximation.[62] Further, we have derived other elastic properties such as the Young's modulus, the Poisson's coefficient, and the shear

TABLE I. Summary of previously reported unit cell parameter ($a_0$) and magnetization of saturation ($M_s$) of greigite, and this work.

| Origin | Grain size (nm) | $a_0$ (Å) | $M_s$ ($\mu_B$ f.u.$^{-1}$) | Reference |
|---|---|---|---|---|
| Natural | 400–500 | 9.876 | ... | 54 |
| Natural | <4–8 ($\mu$m) | 9.87508 ± 72 | 1.06 | 55 |
| Natural | 10–100 ($\mu$m) | 9.859 | ... | 56 |
| Synthetic | <1–44 | 9.872 | 3.12 | 57 |
| Synthetic | 9–13 | 9.83–9.87 | 2.2 ± 0.3 | 13 |
| Synthetic | 10 | ... | 1.04–2.04 | 58 |
| Synthetic | 10–15 | 9.86 | 2.0 ± 0.3 | 12 |
| Synthetic | 30–50 | 9.90 | 1.06–1.27 | 59 |
| Synthetic | ~44 ($\mu$m) | 9.8538(2) | 3.52 ± 0.10 | 18 |
| Synthetic | <150–400 | ... | 0.16–1.54 | 5 |
| ... | ~3 ($\mu$m) | ... | 1.51–2.37 | 60 |
| Computational | Bulk | 9.671 | 3.44 | This paper |

TABLE II. Summary of geometric and electronic properties of bulk $Fe_3S_4$ and $Fe_3O_4$ structures. The properties listed are the mean value of the first-neighbors distance (d), the charge (q), and the spin densities ($m_s$). The sign minus in the spin density represents the antiparallel alignment in the ferrimagnetic spinels.

| | $Fe_3S_4$ bulk | $Fe_3O_4$ bulk |
|---|---|---|
| $d(Fe_{Td})$ (Å) | 2.180 | 1.890 |
| $d(Fe_{Oh})$ (Å) | 2.370 | 2.050 |
| d(S) (Å) | 2.323 | 2.010 |
| $q(Fe_{Td})$ ($e^-$) | 1.1 | 1.8 |
| $q(Fe_{Oh})$ ($e^-$) | 1.0 | 1.7 |
| q(S) ($e^-$) | − 0.8 | − 1.3 |
| $m_s(Fe_{Td})$ ($\mu_B$) | − 2.8 | − 4.0 |
| $m_s(Fe_{Oh})$ ($\mu_B$) | 3.0 | 3.9 |
| $m_s$(S/O) ($\mu_B$) | 0.1 | 0.1 |

TABLE III. Physical properties of $Fe_3S_4$ and $Fe_3O_4$ derived from the elastic constants ($C_{ij}$): bulk modulus (B), shear modulus (G), B/G ratio, Young's modulus (Y), Poisson's ratio ($\sigma$), and anisotropy factor (A). Previously reported $Fe_3O_4$ values are shown for comparison.

| | $Fe_3S_4$ | $Fe_3O_4$ | $Fe_3O_4$ (Expt.) |
|---|---|---|---|
| $C_{11}$ (GPa) | 104.7 | 242.3 | 260.5 ± 1.0[61] |
| $C_{12}$ (GPa) | 41.8 | 159.9 | 148.3 ± 3.0[61] |
| $C_{44}$ (GPa) | 39.0 | 55.0 | 63.3 ± 1.5[61] |
| B (GPa) | 62.8 | 187.4 | 185.7 ± 3.0[61] |
| G (GPa) | 36.0 | 49.5 | 60.3 ± 3.0[61] |
| B/G | 1.7 | 3.8 | 3.1 |
| Y (GPa) | 90.6 | 136.5 | 163.5 |
| $\sigma$ | 0.29 | 0.40 | 0.36 |
| A | 1.24 | 1.34 | 1.13 |

anisotropy factor.[63] The elastic moduli, thus, are useful in predicting the structural stability of materials: the bulk modulus (B), from Eq. (2), represents the resistance to fracture, while the shear modulus (G), from Eq. (3), measures the resistance to a plastic deformation,

$$B = \frac{C_{11} + 2C_{12}}{3}, \tag{2}$$

$$G = \frac{C_{11} - C_{12} + 3C_{44}}{5}. \tag{3}$$

The calculated bulk modulus for $Fe_3S_4$ is 62.8 GPa which is 124.6 GPa smaller than its oxide analogue, whereas the $Fe_3O_4$ bulk modulus differs by only 1.7 GPa from the reported value.[61] The shear modulus is also smaller in $Fe_3S_4$ than in the oxide by 13.5 GPa. These values already depict a $Fe_3S_4$ more deformable than $Fe_3O_4$ also explained by the relationship between B and G, which provides information about the material's fragility/ductility. A ratio of B/G > 1.75 is associated with ductility, whereas a lower value corresponds to a brittle nature.[64] Given a B/G ratio of 1.74 for $Fe_3S_4$ and 3.8 for $Fe_3O_4$ (or 3.1 as derived from Ref. 61), our calculations show that the anionic species in the materials have a significant effect on their properties. $Fe_3S_4$ is harder but more liable to break or shatter compared to the same structure with oxygen as its anion, which is more ductile.

The Young's modulus and Poisson's ratio (Eqs. (4) and (5), respectively) are characteristic properties of a material, related to its elasticity, and are often used to provide a measure of the stiffness of a solid,

$$Y = \frac{9BG}{3B + G}, \tag{4}$$

$$\sigma = \frac{C_{12}}{C_{11} + C_{12}}. \tag{5}$$

The $Fe_3S_4$ Young's modulus is smaller than the one of $Fe_3O_4$ by 45.9 GPa, showing that the $Fe_3S_4$ structure is more susceptible to physical changes than the oxide, which may explain greigite's metastability.[6] Poisson's ratio ($\sigma$) measures the stability of the crystal to shear and provides more information about the interatomic forces than any other elastic property. A Poisson's ratio above 0.25 means that the interaction between atoms is mainly through central forces (with ionic character); whereas lower values indicate that large volume changes occur during uniaxial deformation. A Poisson's ratio below 0.1 is characteristic of covalent materials,[65] this ratio is, therefore, a measure of bond-covalency. The values of $\sigma(Fe_3S_4) = 0.29$ and $\sigma(Fe_3O_4) = 0.40$ show that the governing force between Fe−S atoms in $Fe_3S_4$ is more covalent than in $Fe_3O_4$. This result is in full agreement with the Fe−S orbital overlap in the density of states, see Sec. III C, indicating a higher degree of covalency in $Fe_3S_4$ compared to $Fe_3O_4$.

Elastic anisotropy (A) (Eq. (6)) of a crystal is correlated with the tendency of the material to form micro-cracks. While a perfectly isotropic crystal would have A = 1, we calculate values of $A(Fe_3S_4) = 1.24$ and $A(Fe_3O_4) = 1.34$ indicating that their behaviour slightly depends on the stress direction,

$$A = \frac{2C_{44}}{C_{11} - C_{12}}. \tag{6}$$

The overall description derived from the elastic properties is that greigite is more liable to deformations than $Fe_3O_4$ (small elastic moduli and anisotropy values) and the forces between the ions are more delocalized in the sulfide comparing with a harder anion such as in the oxide magnetite (small Poisson's ratio). As we will show in Sec. III C, the present mechanical description agrees with the description derived from the electronic structure.

### C. Electronic properties

Due to its importance in geomagnetism and environmental magnetic studies, the magnetic behaviour of $Fe_3S_4$ is a major topic in most recent publications on greigite.[1,54,66] We now describe the atomic charges and magnetic moment derived by means of a Bader analysis,[67,68] where the electron (or spin) density associated with each atom is integrated over the Bader volume of the atom in question. The Bader volume is not calculated as a sphere of constant radius due to the changes in the effective atomic radii with the oxidation state of the ion, but it is charge density dependent. Even so, the electron delocalization of the DFT method leads to an underestimation of atomic charges. The mean charges on the octahedral Fe are 1.0 $e^-$ and 1.7 $e^-$, while on tetrahedral Fe they are 1.1 $e^-$ and 1.8 $e^-$ for $Fe_3S_4$ and $Fe_3O_4$, respectively. The magnetization of saturation ($M_s$), i.e., when the magnetization presents its highest possible value and does not increase as a result of an increase in an applied magnetic field, may be predicted from the spin values for the ionic moments according to the Néel model,[26] calculated as the sum of all sublattice moments per formula unit. However, whereas it correctly predicts the $Fe_3O_4$ net magnetization (but not for sublattice moments),[43,69] the $M_s$ of $Fe_3S_4$ is 3.44 $\mu_B$/f.u., smaller than the sum of all its sublattice moments and expected from the Néel model 4.00 $\mu_B$/f.u. The $M_s$ calculated for magnetite is 4.00 $\mu_B$/f.u. in full agreement with the experiment and the Néel model. However, the discrepancy between $M_s(Fe_3S_4)$ and that model is related to the degree of covalency between Fe and the anions: the increased bond-localization of the electrons lowers the ordered magnetic moment. This localization of the *d*-electrons, especially around the octahedral sites, is clearly shown by the states overlapping in the density of states (Fig. 2).

Although $Fe_3O_4$ and $Fe_3S_4$ are structurally equivalent and electronically similar, only the first material undergoes a first-order phase transition, called the Verwey transition, that takes place at temperature $T_V = 122$ K,[70] where the electrical conductivity is decreased on cooling. However, this behaviour is not observed in either natural or synthetic $Fe_3S_4$.[13,24,71] Several attempts have been made to explain the Verwey transformation of $Fe_3O_4$ including: (1) charge order-disorder mechanism in the Fe occupying octahedral positions,[70] (2) crystal-structural transformation that opens a band gap in the electronic band structure[72] that can be seen as a transition from inverted- to normal-spinel,[73] and (3) electron-phonon

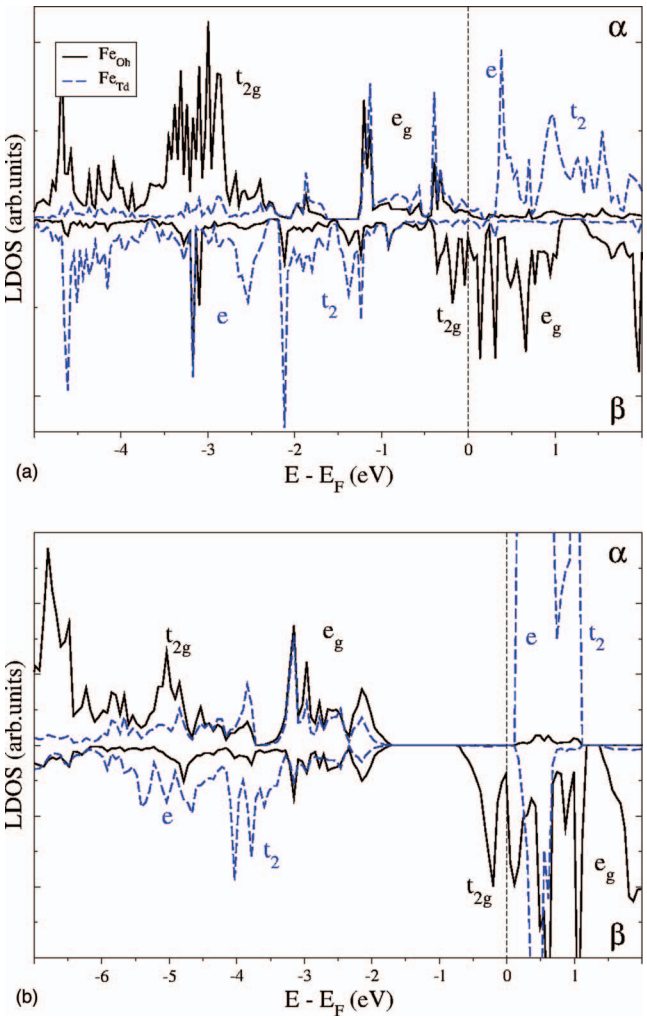


FIG. 2. Density of states of (a) $Fe_3S_4$ and (b) $Fe_3O_4$ projected on octahedral ($Fe_{Oh}$) and tetrahedral ($Fe_{Td}$) iron with respect to the Fermi level (vertical dashed line). Solid-black line describes the octahedral states and dashed-blue line describes the tetrahedral states.

and electron-electron correlations that show a cooperative interplay between lattice, charge, and orbital degrees of freedom.[74] Whereas low-symmetry $Fe_3O_4$ presents a small band gap (~0.14 eV), high-symmetry $Fe_3O_4$ has a continuous band at the Fermi level for the channel of the minority spins $\beta$ indicating half-metallic behaviour, which might be similar for $Fe_3S_4$ despite it is not clear from its DOS. We carried out a hybrid-functional (HSE06) calculation to conclude that the DOS (not shown in the present paper) indicates a similar electronic structure and half-metallic properties than $Fe_3O_4$.

As commented above, the explanation for the covalent character between Fe and S, and the crystal field splitting on Fe atoms, is supported by the projected density of states (LDOS) on $Fe_{Oh}$ and $Fe_{Td}$ (Fig. 2). In both $Fe_3S_4$ and $Fe_3O_4$, the energy difference between the $t_{2g}$ and $e_g$ bands on $Fe_{Oh}$ is about 2 eV and both bands are occupied by majority spin $\alpha$, whereas minority spin $\beta$ partially occupy the $t_{2g}$ from the ferrous states of some $Fe_{Oh}$.[75] However, the oxide bands are shifted down in energy by ~1.5 eV compared with $Fe_3S_4$, again due to the strong oxygen anions. Moreover, the inverse spinel of both minerals disposes an antiparallel spin distribution, the $Fe_{Td}$ majority spin is on $\beta$-bands (e and $t_2$) which are fully occupied. Note, however, that although we have shown here the main trends, higher level calculations are required to represent a pure half-metallic inverse spinel and eliminate spin contamination, as in the $\alpha$-bands from ferric $Fe_{Td}$ electrons.

## IV. CONCLUSIONS

In the present work, we have used the DFT+U approach ($U_{eff}$ = 1 eV for $Fe_3S_4$ and $U_{eff}$ = 3.8 eV for $Fe_3O_4$) to carry out a systematic study of the properties of greigite ($Fe_3S_4$) and its analogue oxide, magnetite ($Fe_3O_4$). The calculated first neighbour distances in the $Fe_3S_4$ material differ by less than 0.1 Å from previous reports. The $Fe_3O_4$ calculated distances are even closer to the benchmark (differences in Fe−O of less than 0.01 Å) for the same type of Fe atoms. However, the average distance between the Fe and the corresponding anion is different enough (~0.3 Å) to provide a clear differentiation between the pure sulfide and the oxide compound, hardly distinguishable in synthetic samples. Furthermore, we have derived a number of mechanical properties from the independent elastic constants $C_{11}$, $C_{12}$, and $C_{44}$ corresponding to $Fe_3S_4$ and $Fe_3O_4$. The ratio of the bulk to shear allowed us to evaluate the effect of the anionic species in the material, i.e., greigite is harder than magnetite, but liable to fracture and Fe−S interaction has a more covalent character than the oxide. Moreover, by comparing the electronic structures, we also found a higher overlapping in S−Fe than in O−Fe, supporting the higher degree of covalency in $Fe_3S_4$ compared to $Fe_3O_4$. The DOS of $Fe_3S_4$ appears more complex since the less electronegative S bands are positioned at higher energy compared to the oxygen bands in $Fe_3O_4$. Furthermore, our theoretical results provide an explanation for the low $Fe_3S_4$ magnetization of saturation, compared to that expected from the Néel model, from both the elastic properties and the DOS analysis. However, a higher level of accuracy, such as hybrid-functional, is required to describe the half-metallic behaviour of $Fe_3S_4$.

## ACKNOWLEDGMENTS

We would like to thank Dr. R. Grau-Crespo for his valuable discussions and comments. In addition, we acknowledge the Engineering and Physical Sciences Research Council (Grant No. EP/H046313) for funding. This work made use of the facilities of HECToR, the UK's national high-performance computing service, which is provided by UoE HPCx Ltd at the University of Edinburgh, Cray Inc, and NAG Ltd, funded by the Office of Science and Technology through EPSRC's High End Computing Programme and provided via our membership of the HPC Materials Chemistry Consortium (EPSRC Grant No. EP/F067496). The authors also acknowledge the use of the UCL@Legion High Performance Computing Facility, and associated support services, in the completion of this work. D.S.-C. thanks UCL for a Graduate Global Excellence Award and an Overseas Research Scholarship from the UCL Industrial Doctorate Centre in Molecular Modelling and Materials Science.

[1]D. Rickard and G. W. Luther, Chem. Rev. **107**, 514 (2007).
[2]S. Hunger and L. G. Benning, Geochem. Trans. **8**, 1 (2007).
[3]R. T. Wilkin and H. L. Barnes, Geochim. Cosmochim. Acta **60**, 4167 (1996).
[4]L. G. Benning, R. T. Wilkin, and H. L. Barnes, Chem. Geol. **167**, 25 (2000).
[5]M. J. Dekkers and M. A. A. Schoonen, Geophys. J. Int. **126**, 360 (1996).
[6]A. R. Lennie, S. A. T. Redfern, P. E. Champness, C. P. Stoddart, P. F. Schofield, and D. J. Vaughan, Am. Mineral. **82**, 302 (1997).
[7]U. Frank, N. R. Nowaczyk, and J. F. W. Negendank, Geophys. J. Int. **168**, 904 (2007).
[8]S. Mann, N. H. C. Sparks, R. B. Frankel, D. A. Bazylinski, and H. W. Jannasch, Nature (London) **343**, 258 (1990).
[9]T. Kasama, M. Posfai, R. K. K. Chong, A. P. Finlayson, P. R. Buseck, R. B. Frankel, and R. E. Dunin-Borkowski, Am. Mineral. **91**, 1216 (2006).
[10]M. Posfai, P. R. Buseck, D. A. Bazylinski, and R. B. Frankel, Am. Mineral. **83**, 1469 (1998).
[11]M. Posfai, P. R. Buseck, D. A. Bazylinski, and R. B. Frankel, Science **280**, 880 (1998).
[12]J. M. D. Coey, M. R. Spender, and A. H. Morrish, Solid State Commun. **8**, 1605 (1970).
[13]M. R. Spender, J. M. D. Coey, and A. H. Morrish, Can. J. Phys. **50**, 2313 (1972).
[14]D. J. Vaughan and J. A. Tossell, Am. Mineral. **66**, 1250 (1981).
[15]K. K. Surerus, M. C. Kennedy, H. Beinert, and E. Munck, Proc. Natl. Acad. Sci. U.S.A. **86**, 9846 (1989).
[16]M. J. Dekkers, H. F. Passier, and M. A. A. Schoonen, Geophys. J. Int. **141**, 809 (2000).
[17]D. J. Vaughan and J. R. Craig, Am. Mineral. **70**, 1036 (1985).
[18]L. Chang, B. D. Rainford, J. R. Stewart, C. Ritter, A. P. Roberts, Y. Tang, and Q. W. Chen, J. Geophys. Res., [Solid Earth] **114** (2009).
[19]D. J. Vaughan and M. S. Ridout, J. Inorg. Nucl. Chem. **33**, 741 (1971).
[20]D. J. Vaughan and J. A. Tossell, Phys. Chem. Miner. **9**, 253 (1983).
[21]M. Braga, S. K. Lie, C. A. Taft, and W. A. Lester, Phys. Rev. B **38**, 10837 (1988).
[22]A. J. Devey, R. Grau-Crespo, and N. H. de Leeuw, Phys. Rev. B **79**, 195126 (2009).
[23]L. Chang, A. P. Roberts, Y. Tang, B. D. Rainford, A. R. Muxworthy, and Q. W. Chen, J. Geophys. Res., [Solid Earth] **113**, B06104, doi:10.1029/2007JB005502 (2008).
[24]A. P. Roberts, Earth Planet. Sci. Lett. **134**, 227 (1995).
[25]L. Neel, J. Phys. Radium **15**, 376 (1954).
[26]L. Neel, Ann. Phys. **3**, 137 (1948).
[27]G. Kresse and J. Hafner, Phys. Rev. B **47**, 558 (1993).
[28]G. Kresse and J. Furthmüller, Comput. Mater. Sci. **6**, 15 (1996).
[29]J. P. Perdew, J. A. Chevary, S. H. Vosko, K. A. Jackson, M. R. Pederson, D. J. Singh, and C. Fiolhais, Phys. Rev. B **46**, 6671 (1992).
[30]S. H. Vosko, L. Wilk, and M. Nusair, Can. J. Phys. **58**, 1200 (1980).
[31]S. Grimme, J. Comput. Chem. **27**, 1787 (2006).
[32]P. E. Blöchl, Phys. Rev. B **50**, 17953 (1994).
[33]N. D. Mermin, Phys. Rev. **137**, A1441 (1965).
[34]B. Zhang, G. A. de Wijs, and R. A. de Groot, Phys. Rev. B **86**, 020406 (2012).
[35]V. I. Anisimov, M. A. Korotin, J. Zaanen, and O. K. Andersen, Phys. Rev. Lett. **68**, 345 (1992).
[36]S. L. Dudarev, G. A. Botton, S. Y. Savrasov, C. J. Humphreys, and A. P. Sutton, Phys. Rev. B **57**, 1505 (1998).
[37]I. D. R. Moreira, F. Illas, and R. L. Martin, Phys. Rev. B **65**, 155102 (2002).
[38]D. Munoz, N. M. Harrison, and F. Illas, Phys. Rev. B **69**, 085115 (2004).
[39]I. Ciofini, F. Illas, and C. Adamo, J. Chem. Phys. **120**, 3811 (2004).
[40]F. Illas and R. L. Martin, J. Chem. Phys. **108**, 2519 (1998).
[41]F. Cora, Mol. Phys. **103**, 2483 (2005).
[42]J. Wang, S. H. Cao, W. Wu, and G. M. Zhao, Phys. Scr. **83**, 045702 (2011).
[43]J. P. Wright, J. P. Attfield, and P. G. Radaelli, Phys. Rev. B **66**, 214422 (2002).
[44]A. Chainani, T. Yokoya, T. Morimoto, T. Takahashi, and S. Todo, Phys. Rev. B **51**, 17976 (1995).
[45]S. Park, T. Ishikawa, and Y. Tokura, Phys. Rev. B **58**, 3717 (1998).
[46]J. H. Park, L. H. Tjeng, J. W. Allen, P. Metcalf, and C. T. Chen, Phys. Rev. B **55**, 12813 (1997).
[47]H. J. Monkhorst and J. D. Pack, Phys. Rev. B **13**, 5188 (1976).
[48]A. J. Devey, R. Grau-Crespo, and N. H. de Leeuw, J. Phys. Chem. C **112**, 10960 (2008).
[49]R. I. Ainsworth, D. Di Tommaso, and N. H. de Leeuw, J. Chem. Phys. **135**, 234513 (2011).
[50]J. Hafner, J. Comput. Chem. **29**, 2044 (2008).
[51]J. A. Morice, L. V. C. Rees, and D. T. Rickard, J. Inorg. Nucl. Chem. **31**, 3797 (1969).
[52]M. E. Fleet, Acta Crystallogr., Sect. B: Struct. Sci. **38**, 1718 (1982).
[53]X. Wu, D. Vanderbilt, and D. R. Hamann, Phys. Rev. B **72**, 035105 (2005).
[54]B. J. Skinner, F. S. Grimaldi, and R. C. Erd, Am. Mineral. **49**, 543 (1964).
[55]V. Hoffmann, Phys. Earth Planet. Inter. **70**, 288 (1992).
[56]F. Giovanoli, Geophys. Res. Lett. **6**, 233, doi:10.1029/GL006i004p00233 (1979).
[57]L. Chang, A. P. Roberts, A. R. Muxworthy, Y. Tang, Q. Chen, C. J. Rowan, Q. Liu, and P. Pruner, Geophys. Res. Lett. **34**, L24304, doi:10.1029/2007GL030302 (2007).
[58]X. Y. Chen, X. F. Zhang, J. X. Wan, Z. H. Wang, and Y. T. Qian, Chem. Phys. Lett. **403**, 396 (2005).
[59]M. Uda, Am. Mineral. **50**, 1487 (1965).
[60]Z. He, S. H. Yu, X. Zhou, X. Li, and J. Qu, Adv. Funct. Mater. **16**, 1105 (2006).
[61]H. J. Reichmann and S. D. Jacobsen, Am. Mineral. **89**, 1061 (2004).
[62]W. Voigt, *Lehrbuch der kristallphysik: (mit ausschluss der kristalloptik)* (B. G. Teubner, 1928).
[63]Y. Wu and W. Hu, Eur. Phys. J. B **60**, 75 (2007).
[64]S. F. Pugh, Philos. Mag. **45**, 823 (1954).
[65]I. R. Shein and A. L. Ivanovskii, Scr. Mater **59**, 1099 (2008).
[66]I. F. Snowball, Phys. Earth Planet. Inter. **68**, 32 (1991).
[67]E. Sanville, S. D. Kenny, R. Smith, and G. Henkelman, J. Comput. Chem. **28**, 899 (2007).
[68]R. F. W. Bader, *Atoms in Molecules - A Quantum Theory* (Oxford University Press, Oxford, 1990).
[69]S. Klotz, G. Rousse, T. Strassle, C. L. Bull, and M. Guthrie, Phys. Rev. B **74**, 012410 (2006).
[70]E. J. W. Verwey, Nature (London) **144**, 327 (1939).
[71]M. Torii, K. Fukuma, C. S. Horng, and T. Q. Lee, Geophys. Res. Lett. **23**, 1813, doi:10.1029/96GL01626 (1996).
[72]G. Rozenberg, M. Pasternak, W. Xu, Y. Amiel, M. Hanfland, M. Amboage, R. Taylor, and R. Jeanloz, Phys. Rev. Lett. **96**, 045705 (2006).
[73]M. P. Pasternak, W. M. Xu, G. K. Rozenberg, R. D. Taylor, and R. Jeanloz, J. Magn. Magn. Mater. **265**, L107 (2003).
[74]P. Piekarz, K. Parlinski, and A. M. Oles, Phys. Rev. B **76**, 165124 (2007).
[75]M. Fonin, R. Pentcheva, Y. S. Dedkov, M. Sperlich, D. V. Vyalikh, M. Scheffler, U. Rudiger, and G. Guntherodt, Phys. Rev. B **72**, 104436 (2005).